Hybrid Approach for the Modeling of Magnetic Force Excitations in Multipole Wind Turbine Generators Considering Air Gap Imperfections

Kern, Alexander ; Mulder, Christoph ; Hameye, Kay ; Dong, Jianning

DOI
10.1109/ECCE47101.2021.9595358

Publication date
2021

Document Version
Final published version

Published in
2021 IEEE Energy Conversion Congress and Exposition (ECCE)

Hybrid Approach for the Modeling of Magnetic Force Excitations in Multipole Wind Turbine Generators Considering Air Gap Imperfections

Alexander Kern, Christoph Mülder, Kay Hameyer
Institute of Electrical Machines (IEM)
RWTH Aachen University
Aachen, Germany
alexander.kern@iem.rwth-aachen.de

Jianning Dong
Department of DC Systems, Energy Conversion and Storage
TU Delft
Delft, The Netherlands
J.Dong-4@tudelft.nl

2021 IEEE Energy Conversion Congress and Exposition (ECCE) | 978-1-7281-5135-9/21/$31.00 ©2021 IEEE | DOI: 10.1109/ECCE47101.2021.9595358

***Abstract*—Magnetic force excitations in the air gap of generators can lead to tonal noise emissions of direct-drive wind turbines. Besides the magnetic circuit design, the generator air gap topology has an impact on the excited vibration modes and their frequencies, respectively. For the model-based analysis of the excited force density waves, the spatial and temporal distribution of the air gap magnetic flux density has to be modeled accurately, since it is directly linked with the interfacial forces by the Maxwell stress tensor. Electromagnetic simulations by finite elements consider nonlinear effects, as e.g. saturation, and are therefore convenient for the quantitative analysis. The processing of finite element meshes for the stated purpose is however cumbersome, since many full-models of huge structures (multipole) are necessary. Semi-analytical approaches using conformal maps are efficient for analyzing air gap deformations linearly, even though they do not consider the saturation behavior implicitly. In this work, an efficient hybrid approach for the modeling of force excitations by multipole generators considering air gap imperfection is presented. The calculation method combines electromagnetic 2D-finite-element results of symmetrical units with permeance functions of deformed air gaps obtained by conformal mapping to study the spatial and temporal shape of excited force density waves along the whole generator circumference.**

***Index Terms*—Generators, Acoustic Emission and Vibration, Modeling, Air Gap Imperfections, Nonuniform Air Gap**

I. Introduction

The design and analysis of mechatronic systems require holistic model approaches. In case of wind turbines, this assumption means that models have to consider a coupling between e.g. electromagnetic, mechanical (e.g. structural dynamic) and thermal phenomena. Using the example of air gap topologies of direct-drive generators, it is evident that this interaction is pronounced: Eccentricity caused by unbalanced pull exerted at the wind rotor or thermal expansion due to the dissipation of ohmic loss energy of electrical currents lead to a deformation of the air gap. According to Ampère's circuit law, the magnetic flux density depends on the local air gap width. Since magnetic forces occurring at material transitions adjacently to the air gap are directly correlated with it, the shape and amplitude or rather the spatial and temporal distribution of those force excitations are affected. This may result in turn to a deviation of the rated operational behavior predicted in the course of the design process: The vibrational as well as acoustic characteristics of the wind turbine change. Related to their low-speed and high-torque design, gearless wind turbine generators are multipole synchronous machines [1]. The finite element (FE) based electromagnetic analysis of the entire topology is very cumbersome. Therefore, partial models representing a symmetrical unit of the machine assuming ideal or uniform air gap conditions are usually solved. When studying air gap imperfections, the smallest symmetrical unit might be the full geometry in case of an asymmetric deformation. Particularly eccentricity, that can occur statically and dynamically, is under the scope of electrical machine studies in terms of unbalanced magnetic pull or additional excited vibration modes [2]. Semi-analytical modeling approaches based on conformal maps are motivated to consider both, the aforementioned effects and the intrinsic geometry of rotating electrical machines, as e.g. the slotted magnetic flux leading core, qualitatively [3]. Nevertheless, these approaches assume a linear material behavior that is equivalent to infinite permeable electrical steel. Magnetic saturation is consequently neglected. Direct-drive wind turbine generators are designed to operate in saturated state. It saves material and therefore reduces the weight of the generator which has a high proportion of the total nacelle weight in those applications. This work presents an efficient hybrid modeling approach combining numeric and semi-analytic models to consider both impacts,

- arbitrary air gap deformations,
- nonlinear material behavior (saturation) on the spatial and temporal distribution of magnetic force excitations.

In chapter 2, magnetic field- and force calculation methods of electrical machines, namely conformal mapping (CM), finite element method (FEM) and the Maxwell stress tensor formulation are presented. Based on these methods, the hybrid modeling (HM) is derived and evaluated exemplary for no-load and loaded operation conditions in chapter 3. The results are concluded and an outlook for future studies is given in the last chapter 4.

II. 2D-Magnetic Field and Force Calculation Methods of Electrical Machines

A. Conformal Mapping

Conformal mapping is used to transform a complex geometrical setup, as e.g. the topology of an electrical machine, into a specific geometrical shape. An electromagnetic field problem is then solved in this simplified geometry by using analytical functions [4]. The inverse transformation gives the desired field quantities in the original machine topology. The mathematical fundament of conformal maps are holomorphic permeance functions that describe the transformation of the geometry [5].
In [6] an analytical description of a magnetic scalar potential Ω, which is caused by a line current that is located between two infinite permeable concentric cylinders with a constant distance, is presented. Based on this potential formulation, the spatial and temporal distribution of the air gap magnetic flux density can be derived. The transformation to this annular geometry is performed with the aid of three conformal maps presented below [7]. Due to the geometrical setup, it is sufficient to only model one rotor and stator pitch respectively.

1) s-to z-plane (Logarithmic Mapping): All characteristic points of the original geometry of one rotor pole or stator slot are described by a radius R from the center of the machine and an angle α towards the horizontal axis:

$$s = R \cdot e^{\mathrm{j}\alpha}. \tag{1}$$

For the transformation to the z-plane the function

$$z = f(s) = \log s = \log R + \mathrm{j}\alpha \tag{2}$$

is used. The function $f(s)$ represents a rectification of the rotor and stator geometry respectively.

2) z- to w-plane (Schwarz-Christoffel Mapping): With the aid of the Toolbox by T. Driscoll [8] all points in the z-plane are transformed into the w-plane, where the rotor and stator geometry are represented by two opposing rectangles. The exact functional context of the transformation function cannot be stated in a closed form since an integral expression is solved numerically [6].

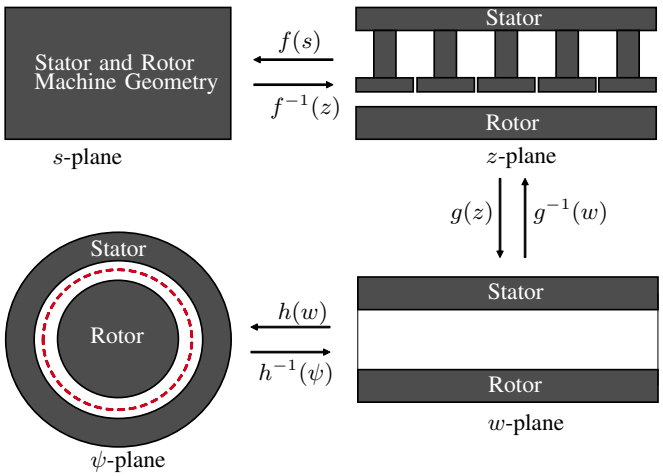

Fig. 1. Schematic flow chart of the transformation of the geometry.

3) w- to ψ-plane (Exponential Mapping): The geometrical points in the ψ-plane can be described by the conformal map [9]

$$\psi = h(w) = \exp\left(\frac{\tau}{\Delta V} \cdot \left(w + \frac{\Delta U}{2}\right)\right). \tag{3}$$

In (3) τ denotes the angle of one pole pitch or one slot pitch. The variables ΔU and ΔV depend on the geometric properties in the w-plane [10]. Since the mapped geometry has now the aforementioned cylindrical shape (see figure 1), the magnetic scalar potential Ω in the air gap, denoted by the red dashed line in figure 1, can be calculated with the potential formulation stated in [6]. Hereby, each winding with a current I is transformed into an infinitely long line current at a certain fixed position in the air gap. The corresponding radial and tangential component of the air gap magnetic flux density are given by

$$\vec{B}_\delta = -\mu_0 \cdot \nabla\Omega = B_{\delta,\mathrm{rad}} \cdot \vec{e}_{\mathrm{rad}} + B_{\delta,\mathrm{tan}} \cdot \vec{e}_{\mathrm{tan}}. \tag{4}$$

In order to transform the magnetic scalar potential from the ψ-plane to the s-plane, a complex valued permeance function $\underline{\lambda}$ is defined that describes the mapping of the geometry:

$$\underline{\lambda} = \left(\frac{\partial\psi}{\partial w} \cdot \frac{\partial w}{\partial z} \cdot \frac{\partial z}{\partial s}\right) \cdot \frac{1}{\lambda_0} = \lambda_{\mathrm{rad}} + \mathrm{j}\lambda_{\mathrm{tan}}. \tag{5}$$

The real part is defined as the radial component and the imaginary part as the tangential component. The conformal transformation of the topology leads to a scaling of the geometric properties. For this reason, a real valued permeance function λ_0 is introduced. It describes the transition from the slotless geometry in the original s_0-plane to the ψ-plane [10].

$$\lambda_0 = \left(\frac{\partial\psi}{\partial w} \cdot \frac{\partial w}{\partial z} \cdot \frac{\partial z}{\partial s_0}\right). \tag{6}$$

The resulting permeance function $\underline{\lambda}$ describes the transition of the air gap magnetic flux density $\underline{B}_{\delta,\psi}$ from a cylindrical slotless air gap geometry towards the magnetic flux density $\underline{B}_{\delta,\mathrm{s}}$ in a slotted geometry [11]:

$$\underline{B}_{\delta,\mathrm{s}} := B_{\delta,\mathrm{rad}} + jB_{\delta,\mathrm{tan}} = (B_{\delta,\psi,\mathrm{rad}} + \mathrm{j}B_{\delta,\psi,\mathrm{tan}}) \cdot (\lambda_{\mathrm{rad}} + \mathrm{j}\lambda_{\mathrm{tan}})^*. \tag{7}$$

The permeance function can be evaluated physically and geometrically. From the geometric point of view, the permeance describes the conformal transformation of the slotted stator with $\underline{\lambda}_{\mathrm{S}}$ and the sinus pole rotor geometry with $\underline{\lambda}_{\mathrm{R}}$ respectively. It defines in which way the radial and tangential component of the air gap magnetic flux density change by the effect of stator slotting and the presence of rotor poles. Based on the physical definition

$$\lambda \propto \frac{\Theta}{\Phi} \tag{8}$$

is valid, where Φ is the magnetic flux and Θ is the magnetomotive force correlating with the electrical current. Therefore,

the permeance quantifies how much magnetic flux at a certain magnetomotive force can pass a geometric unit.

B. Finite Element Method

For complex geometries, like slotted rotating field electrical machines, a direct analytical solution of the local magnetic field by Maxwell's equation is not possible. Therefore, the considered domain, on which the field solution should be obtained, is subdivided into small segments of triangles that are called finite elements.
For the quasistatic case, the magnetic vector potential $\vec{A}$ is solved at every node of each triangle [12]:

$$\nabla \times \left(\nu \nabla \times \vec{A} \right) = \vec{J}_{\mathrm{s}}. \tag{9}$$

The vector source current density of the coils is denoted by $\vec{J}_{\mathrm{s}}$ and ν is the highly nonlinear reluctivity of the electrical steel. Based on the obtained magnetic vector potential the magnetic flux density can be determined on the complete solution domain with

$$\vec{B} = \nabla \times \vec{A}. \tag{10}$$

In the following, FE-simulations are conducted by an in-house software environment.

C. Magnetic Air Gap Forces

Based on the spatial and temporal distribution of the air gap magnetic flux density, the electromagnetic force excitation in the generator can be calculated. For 2D-problems follow from the Maxwell stress tensor both the radial and tangential force density formulation:

$$\sigma_{\mathrm{rad}}\left(\phi, t\right) = \frac{{B_{\delta,\mathrm{rad}}}^2\left(\phi, t\right) - {B_{\delta,\mathrm{tan}}}^2\left(\phi, t\right)}{2\mu_0}, \tag{11}$$

$$\sigma_{\mathrm{tan}}\left(\phi, t\right) = \frac{B_{\delta,\mathrm{rad}}\left(\phi, t\right) \cdot B_{\delta,\mathrm{tan}}\left(\phi, t\right)}{\mu_0}. \tag{12}$$

Analog to the air gap magnetic flux density, the magnetic forces are a function of the circumferential position and time. Using a 2D-Fourier transformation (2D-FFT), their periodicity in time and space can be analyzed [13]. The spatial dimension is linked to the circumferential angle ϕ and indicates the mode number. The frequency of the propagating force wave depends on its temporal periodicity during one mechanical rotation.

D. Evaluation of Field Calculation Methods

CM offers the possibility to model diverse 2D-geometries by the definition of permeance functions. It allows the consideration of changing geometric properties by recalculating the permeance functions very efficiently. The semi-analytical calculation approach using conformal transformations describes the air gap magnetic flux density composed in its radial and tangential component that can be used to derive the corresponding magnetic force densities. The major disadvantage is that magnetic saturation is not considered since rotor and stator iron are assumed to be infinite permeable. For this reason, occurring nonlinear effects cannot be described. FEM represents an accurate modeling of electrical machines with complex 2D-and 3D-geometries. A holistic solution of the electromagnetic field quantities is obtained, since the consideration of the material characteristic $B(H)$ of the rotor and stator iron allows to evaluate the effect of magnetic saturation on the air gap magnetic flux density. The main drawback is the cumbersome preprocessing and the processing itself that are the creation of several models and meshes of the machine to account for different air gap imperfections and the corresponding calculation times, respectively. These disadvantages are particularly pronounced for multipole synchronous machines, as those used in gearless wind turbines, whose full-models involve even higher computational efforts.
In order to analyze the plane effect of air gap imperfections, the use of conformal maps is preferable. The crucial advantage is that the geometrical deformed air gap topology can be modeled separately. The change of the air gap width along the circumference $\delta(\phi)$ can be described by an own permeance function $\lambda_{\mathrm{Deformation}}$ that is defined as

$$\lambda_{\mathrm{Deformation}}(\phi, t) = \frac{\delta_0}{\delta(\phi, t)}, \tag{13}$$

where δ_0 is the nominal air gap width and $\delta(\phi, t)$ denotes the air gap width function of the deformed topology [2]. The total air gap describing permeance function is then given by the product of the individual geometry describing permeance functions

$$\underline{\lambda}_{\delta}\left(\phi, t\right) = \underline{\lambda}_{\mathrm{R}}\left(\phi, t\right) \cdot \underline{\lambda}_{\mathrm{S}}\left(\phi, t\right) \cdot \lambda_{\mathrm{Deformation}}(\phi, t). \tag{14}$$

Therefore, the spatial and temporal distribution of the air gap magnetic flux density is affected by the deformation permeance function by multiplication according to (7) in the conformal mapping approach. The real valued property of the deformation permeance function also implies that any nonlinear effect due to an air gap imperfection is neglected intrinsically.

III. Hybrid Modeling Approach

In the hybrid modeling approach solutions from CM and FEM are combined. The basic idea is to keep the advantage of CM to describe air gap imperfections efficiently. The impact of magnetic saturation on the air gap magnetic flux density, calculated with CM, is considered by a complex valued function $\underline{\chi}_{\mathrm{sat}}$ which is parameterized by FE-solutions.

A. Comparison of FEM and CM

Figure 2 and figure 3 show for two different rotor excitation currents $i_{\mathrm{f},1} = 0.1 \cdot i_{\mathrm{f,N}}$ and $i_{\mathrm{f},2} = i_{\mathrm{f,N}}$ and the nominal air gap width under no-load operation the course of the radial component of the air gap magnetic flux density over two pole pitches at a fixed time instant using CM and FEM. From figure 2 follows that both calculation methods lead to a similar result concerning amplitude and shape when the influence of magnetic saturation is negligible. Ignoring the effect of magnetic saturation leads to an error of the amplitude of the air gap magnetic flux density. By the use of CM, the peak value

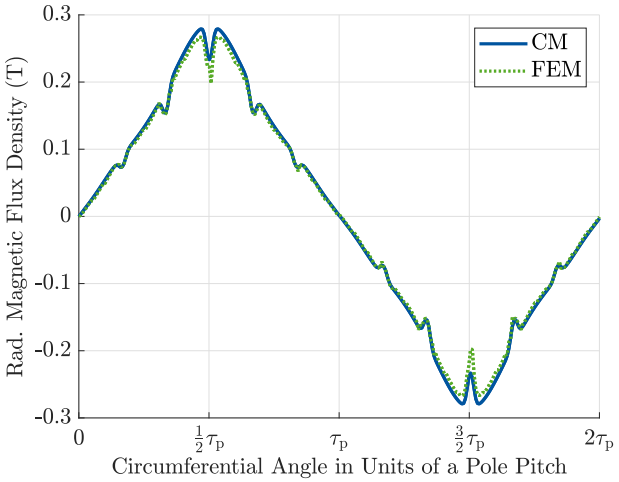

Fig. 2. Comparison of the radial component of the air gap magnetic flux density calculated with CM and FEM in no-load operation at an excitation state of $i_\mathrm{f} = i_{\mathrm{f},1}$.

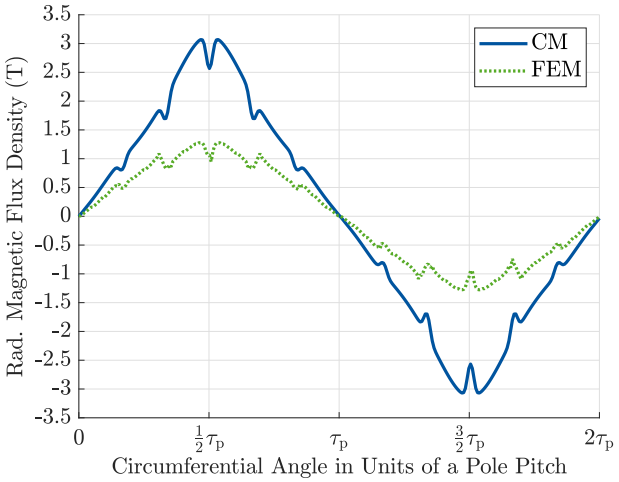

Fig. 3. Comparison of the radial component of the air gap magnetic flux density calculated with CM and FEM in no-load operation at an excitation state of $i_\mathrm{f} = i_{\mathrm{f},2}$.

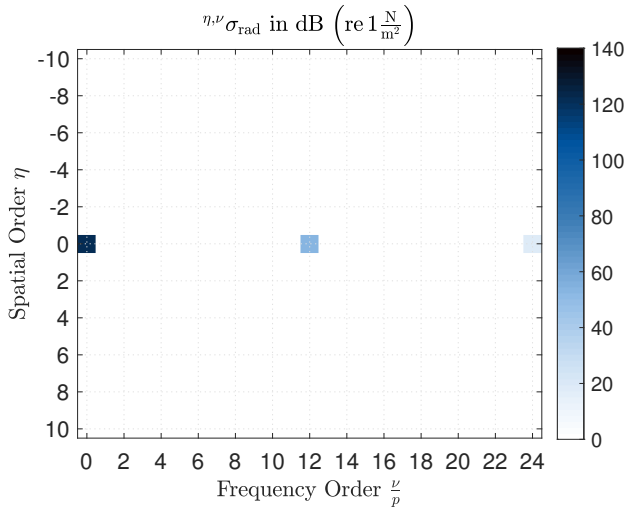

Fig. 4. Spectrum of the radial force density calculated by CM in no-load operation at an excitation state of $i_\mathrm{f} = i_{\mathrm{f},2}$.

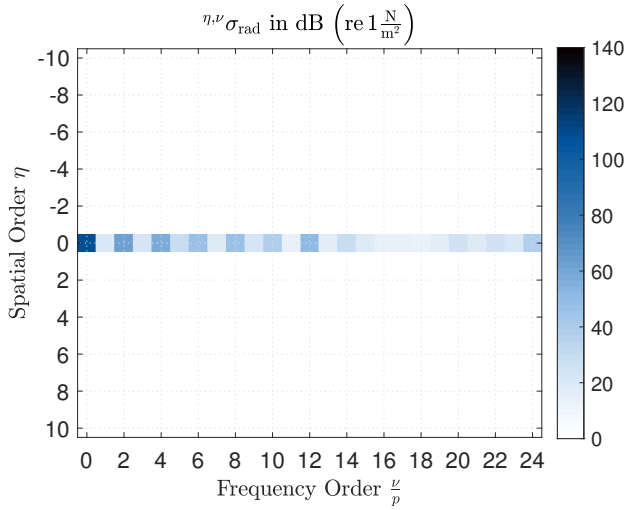

Fig. 5. Spectrum of the radial force density calculated by FEM in no-load operation at an excitation state of $i_\mathrm{f} = i_{\mathrm{f},2}$.

is unphysically high. Moreover, magnetic saturation influences the shape and by this, the harmonic content of the air gap magnetic flux density and the linked magnetically excited force waves (see figure 3).

Figure 4 and figure 5 show the 2D-FFT of the radial force density on a logarithmic scale using CM and FEM over $\eta = \pm 10$ spatial and $\frac{\nu}{p} = 24$ frequency orders. The frequency orders are normalized to the pole pair number p for sake of a wide-ranging representation. By the comparison of the spectra, it can be seen that the saturation of the iron changes the magnetic force spectrum in terms of additional frequency orders. Subsequently, two differences in the results of the semi-analytical approach occur compared to those of FEM:

- additional frequency orders are excited in accordance with reference [14] and
- the amplitudes of the force waves are overestimated.

Therefore, CM in this form is not well suited in order to analyze the excited magnetic forces in saturated operating states.

B. Model Parametrization

The decreasing permeability of electric steel, that is the capability of conducting magnetic flux at a certain magnetomotive force, at magnetic flux densities beyond $B \approx 1$ T has the consequence that an increase of the electromagnetic excitation cannot be transferred linearly into a rise of the magnetic flux density. Referring to (8), the general idea is to adjust the air gap permeance function. Influencing parameters are the air gap width at a certain circumferential position

and time instant as well as the applied magnetomotive force according to the relation

$$B_\delta \propto \frac{\Theta}{\delta}. \tag{15}$$

In [7] it is suggested for considering magnetic saturation to fictively enlarge the air gap under each tooth based on the magnetic voltage drops in the neighboring teeth and the yoke. In the case of a multipole direct-drive generator, this procedure would increase the calculation time significantly since for every time step a nonlinear system of equation has to be solved and the corresponding values of the magnetic field strengths have to be interpolated. Another disadvantage of this methodology is that, in the case of air gap imperfections, the air gap width under each tooth is not constant. A magnetic circuit modeling approach presented in [15] would also assume a uniform air gap width under each tooth. Moreover, the physically correct value of the average magnetic flux density in the stator teeth has to be available.

In order to adjust the original air gap permeance function in no-load operation, a complex valued saturation permeance function is defined:

$$\begin{aligned}\underline{\chi}_{\mathrm{sat}} &= \frac{\underline{B}_{\delta,\mathrm{FEM}}\left(i_\mathrm{f}, t, \phi, \delta\right)}{\underline{B}_{\delta,\mathrm{CM}}\left(i_\mathrm{f}, t, \phi, \delta_0\right)} \\ &= \chi_{\mathrm{sat,rad}}\left(i_\mathrm{f}, t, \phi, \delta\right) + \mathrm{j}\chi_{\mathrm{sat,tan}}\left(i_\mathrm{f}, t, \phi, \delta\right).\end{aligned} \tag{16}$$

The data basis of the parametrization of the saturation permeance function are FE-field solutions of the air gap magnetic flux density. The field solutions are obtained

- over one field periodicity for the symmetric geometry (e.g. a double pole pitch),
- for a given set of excitation currents i_f and
- at equally spaced constant air gap widths δ over one field periodicity.

Figure 6 illustrates an excerpt of the radial component of the saturation permeance function calculated at the nominal excitation current and the nominal air gap width. The circumferential points with a rather constant value indicate the location of a stator tooth. An increased saturation state is linked to a decreasing value of the saturation permeance function. The high harmonic content in the saturation permeance function emphasizes the nonlinear relation between magnetomotive force and the spatial distribution of the air gap magnetic flux density, which is neglected by the conformal mapping approach. The dependency on time and space of the saturation permeance function is due to the fact that at a fixed circumferential position, the saturation state in the iron changes with the revolution of the rotor. Likewise, at a fixed time instant, the saturation state of the teeth along the circumference is different. For the calculation of the spatial and temporal distribution of the air gap magnetic flux density in case of a non-uniform air gap topology, the saturation permeance function becomes a look-up table (LUT). For a fixed excitation current $i_{\mathrm{f,set}}$ and for each time step t_{set}, the air gap width δ at each circumferential position ϕ_{set} is the input parameter to the LUT. A complex value of $\underline{\chi}_{\mathrm{sat}}$ is interpolated

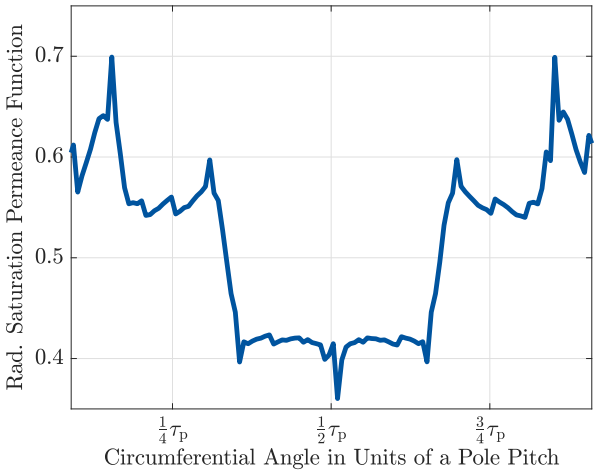

Fig. 6. Excerpt of the radial component of the saturation permeance function at an excitation state of $i_\mathrm{f} = i_{\mathrm{f},2}$ and the nominal air gap width.

and multiplied to the value of the air gap magnetic flux density $\underline{B}_{\delta,\mathrm{CM}}\left(i_{\mathrm{f,set}}, t_{\mathrm{set}}, \phi_{\mathrm{set}}, \delta_0\right)$ obtained by CM at the nominal air gap width. This procedure is applied for all time steps and all spatial discretization points along the air gap circumference. The air gap magnetic flux density using HM is obtained in an arbitrary deformed air gap shape by

$$\begin{aligned}&\underline{B}_{\delta,\mathrm{HM}}\left(i_{\mathrm{f,set}}, t_{\mathrm{set}}, \phi_{\mathrm{set}}, \delta\right) = \\ &\underline{B}_{\delta,\mathrm{CM}}\left(i_{\mathrm{f,set}}, t_{\mathrm{set}}, \phi_{\mathrm{set}}, \delta_0\right) \cdot \underline{\chi}_{\mathrm{sat}}.\end{aligned} \tag{17}$$

Figure 7 shows the flow chart of the procedure for determining the complex factor $\underline{\chi}_{\mathrm{sat}}$ and the force densities originating from the air gap magnetic flux density calculated with HM. The circumferential varying air gap width changes the saturation sate in the rotor and stator iron. The saturation permeance function is parametrized by an arbitrary air gap deformation and is, therefore, not constant but dependent on the circumferential change of the air gap width. In conclusion, HM is a reconstruction of the air gap magnetic flux density calculated with FEM for circumferential varying air gap widths evaluated in the middle between rotor and stator. The basis

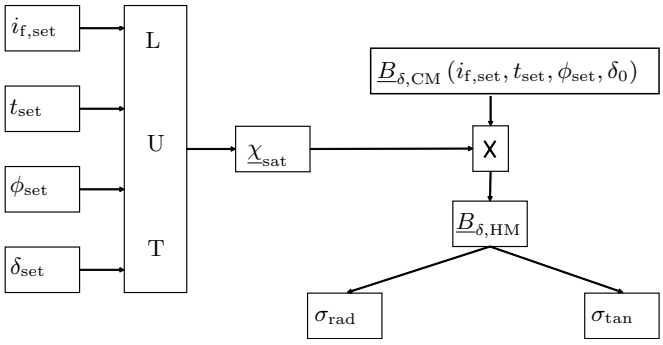

Fig. 7. Methodology to identify the complex number $\underline{\chi}_{\mathrm{sat}}\left(i_{\mathrm{f,set}}, t_{\mathrm{set}}, \phi_{\mathrm{set}}, \delta_{\mathrm{set}}\right)$ and to calculate the resulting force densities.

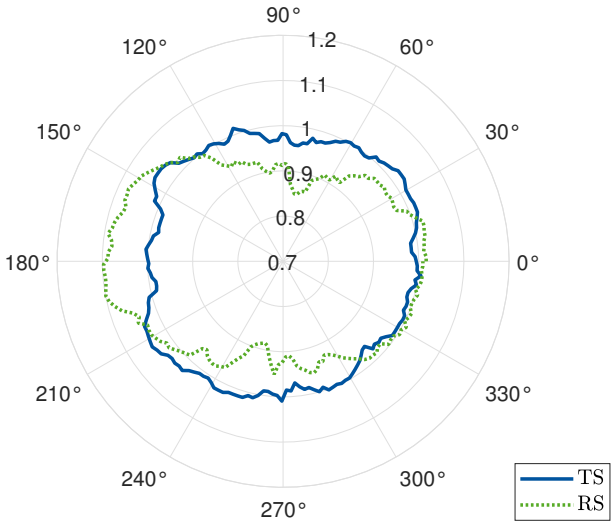

Fig. 8. Normalized air gap width functions at the tower side (TS) and rotor hub side (RS).

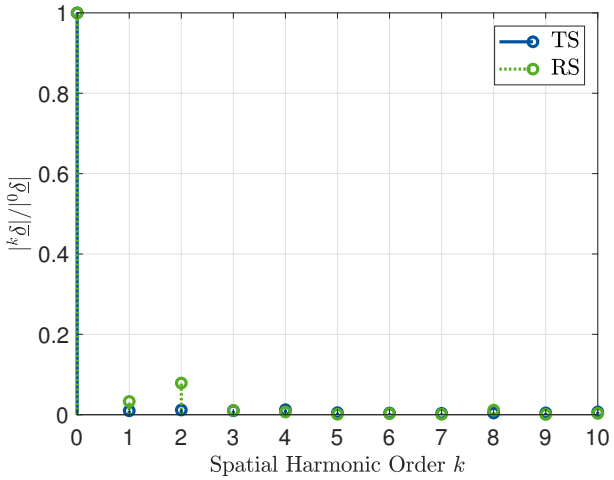

Fig. 9. Normalized spatial spectra of the air gap width functions at the tower side (TS) and rotor hub side (RS).

of the reconstruction is the air gap magnetic flux density at the same magnetomotive force and the nominal air gap width calculated with CM.

IV. Application of HM

The hybrid modeling approach is applied in order to analyze the radial and tangential force excitation in no-load and full-loaded constant power operation region, assuming a purely sinusoidal current stator excitation, for an experimentally measured air gap imperfection.

A. Measured Air Gap Shapes

Figure 8 shows the measured air gap width functions at the tower side (TS) and rotor hub side (RS) normalized to the mean value of the air gap width function at TS. The air gap width is read out by a sensor on the rotor during one mechanical rotation. Therefore, the air gap deformation is static meaning that the air gap width function $\delta(\phi)$ is only dependent on the circumferential position and not the time instant. The extent and shape of the air gap imperfections varies from TS to RS significantly.

The spatial Fourier decomposition of the air gap width functions at RS and TS normalized to their respective mean value is shown in figure 9. The Fourier decomposition of the air gap width function enables to detect and analyze the shape of the specific imperfection. At RS, the air gap has an oval shape compared to TS. Moreover, the non-null spatial harmonic order $k = 1$ indicates a slight eccentric rotor position, whereas the harmonic order $k = 2$ correlates with the oval air gap shape. Higher spatial harmonic orders are related to

- randomly distributed manufacturing tolerances of the active materials or
- thermally induced rotor or stator deformations.

The latter imperfection type is motivated by the specific fixing of the stator and rotor in the wind turbine [16]. At elevated temperatures, the active materials bulge between the fixings. The symmetry of the resulting air gap shape and therefore the predominant spatial harmonic order in the air gap width function is directly linked with the number of carrier arms.

B. Analysis of Electromagnetic Force Excitations in Deformed Air Gaps

As an example application of HM, the impact of the deformed air gap shape at RS on the electromagnetic force excitation is studied.

1) No-Load Operation: The methodology shown in figure 7 is used to calculate the spatial and temporal distribution of the electromagnetic force excitations in the radial direction at the nominal excitation current. Figure 10 illustrates the spatial distribution of the resulting air gap magnetic flux density. Compared to the CM approach, the spatial distribution is not just linearly scaled with the deformation permeance function and the peak amplitudes remain in physically sensible boundaries determined by the saturation state. Figure 11 shows the 2D-FFT of the radial force density up to twice the slot harmonic frequency order $\frac{\nu}{p} = 24$. The spatial orders $\eta = 1, 2, 4$ are primarily related to the ovalization and the slight eccentric rotor position. Excited force waves of higher spatial orders are due to mutual convolutions of non-null harmonic orders in the air gap width function and possibly numerical noise caused by the interpolation methodology.

2) Full-Loaded Operation: In full-loaded operation, the superposition of the separately calculated stator and rotor field in the middle of the air gap, as it is assumed by CM, does not lead to a physically correct distribution of the air gap magnetic flux density. The reason could be a saturation state dependent parametrization of the rotor permeance function under the presence of a stator field. Hence, the saturation permeance function from (6) is purely mathematical. In this case, the spatial and temporal distribution of the air gap magnetic flux density is determined by the direct interpolation

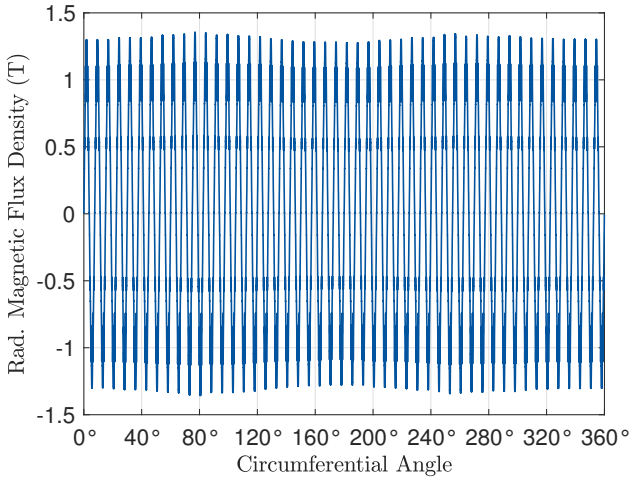

Fig. 10. Spatial distribution of the air gap magnetic flux density at RS calculated with HM in no-load operation at the nominal rotor excitation state.

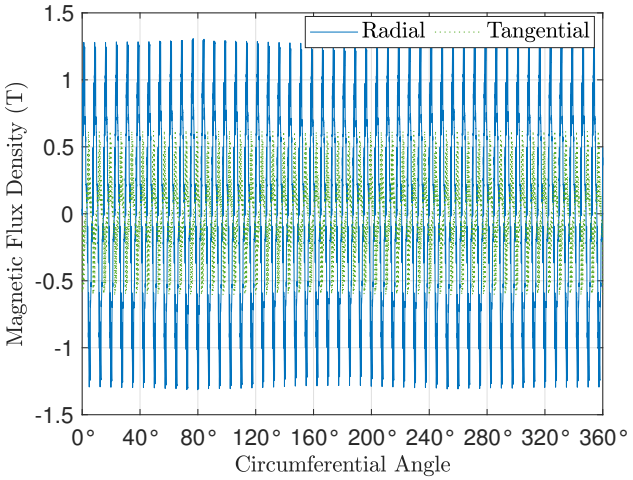

Fig. 12. Spatial distribution of the air gap magnetic flux density at RS calculated with HM in full-loaded operation.

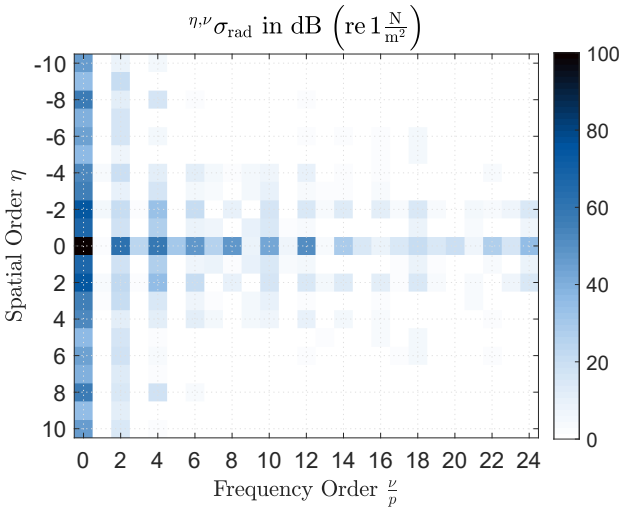

Fig. 11. Excerpt of the spectrum of the radial force density at RS calculated with HM in no-load operation at the nominal rotor excitation state.

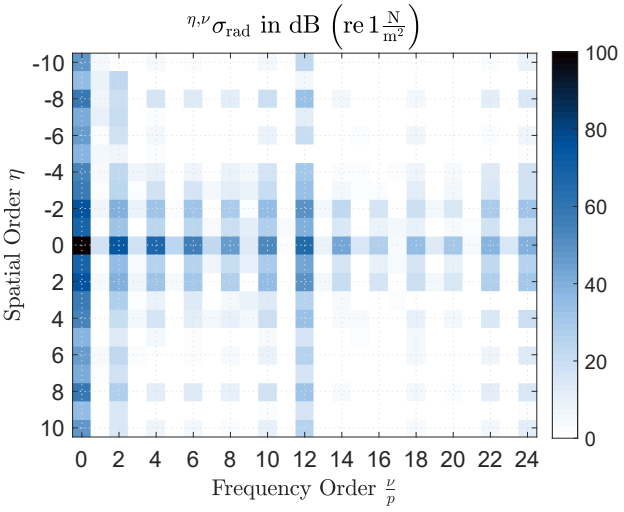

Fig. 13. Excerpt of the spectrum of the radial force density at RS calculated with HM in full-loaded operation.

between the corresponding FE-solutions. The input parameters to the LUT are extended by the stator current components at the considered operating point. Nevertheless, the original HM methodology can also be applied to the here mathematically defined saturation permeance function either way.

Figure 12 illustrates the spatial distribution of the radial and tangential component of the resulting air gap magnetic flux density. The rotor excitation and the related stator current are so high such that the saturation state remains nearly unchanged even at an increase or decrease of the air gap width. Hence, the effect of the circumferential varying air gap width is damped by the magnetic saturation of the rotor and stator iron. In full-loaded operation the peak value of the tangential component of the air gap magnetic flux density is approximately one half of the radial one. In consequence, the tangential force waves with spatial orders $\eta \neq 0$ contribute to the structural dynamic excitation of the stator core, additionally [17] [18].

Figures 13 and 14 show the 2D-FFT of the radial and tangential force density up to twice the slot harmonic frequency order. The spectra of the radial force density in no-load and full-loaded operation especially differ in the amplitudes of components with the first slot harmonic frequency order $\frac{\nu}{p} = 12$.

V. Conclusion and Outlook

A novel hybrid modeling approach, that allows to describe and analyze the impact of magnetic saturation on the dynamic force excitation in a multipole electrical machine efficiently, is presented. It combines the advantages of the semi-analytical CM and the numerical finite-element-based calculation approaches. Time consuming FE-simulations only have to be

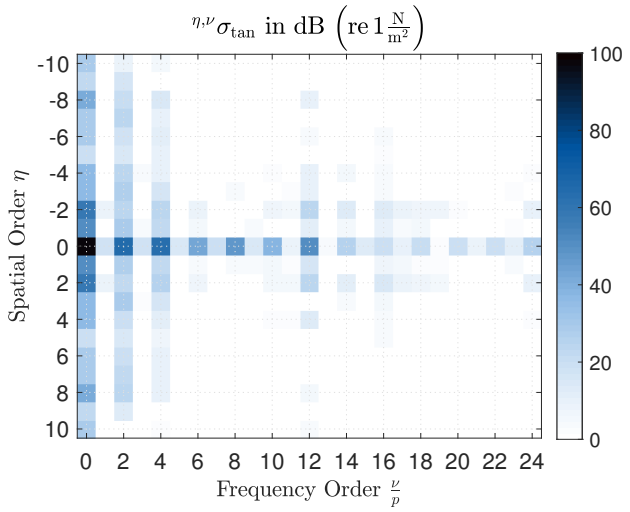

Fig. 14. Excerpt of the spectrum of the radial force density at RS calculated with HM in full-loaded operation.

carried out over one symmetrical unit of the machine at different but constant air gap widths at the studied operational points.In case of wind turbine generators, these are based on characteristic curves derived in the design process.

The HM-approach considers the nonlinear material behavior of iron by the adjustment of the air gap permeance function based on the saturation state of the machine. In contrast to the FEM, no holistic solution of the electromagnetic field problem is obtained. Analogously to CM, only the spatial and temporal distribution of the air gap magnetic flux density is calculated, which is almost sufficient to analyze the electromagnetic force excitation. The simulation and calculation time are, when compared to FEM, significantly reduced. Nevertheless, the influence of magnetic saturation on the electromagnetic force excitation under the influence of an air gap imperfection can be modeled and described with plausible and quantifiable results. The HM approach is motivated for multipole machines as direct-drive synchronous generators in wind turbines. The reconstruction of the air gap magnetic flux density relies on the here valid assumption that the air gap width difference for physically sensible air gap deformations between rotor poles, through which the magnetic flux paths are closed, is negligible small. Due to the nonlinearity of the distribution of the air gap magnetic flux density, a shape preserving piecewise interpolation method may be used [19]. It is further thought that the efficiency of HM can be increased and the slight numerical noise in the spectra of the force densities, occurring especially for unsymmetrical deformations, can be reduced by the use of Chebyshev nodes for the choice of the grid points for the reference solution of the air gap magnetic flux density calculated with FEM. The validation of those assumptions as well as a comparison to full model FE-solutions, also considering deformed air gaps in 3D, is the matter of ongoing research.

REFERENCES

[1] H. Polinder, F. F. A. van der Pijl, G. -. de Vilder and P. J. Tavner, "Comparison of direct-drive and geared generator concepts for wind turbines," in IEEE Transactions on Energy Conversion, vol. 21, no. 3, pp. 725-733, Sept. 2006.

[2] A. Ruf, M. Schröder, A. Putri, D. Franck and K. Hameyer, "Analysis and determination of mechanical bearing load caused by unbalanced magnetic pull," 2014 17th International Conference on Electrical Machines and Systems (ICEMS), 2014, pp. 8-14.

[3] Z. Zhu and D. Howe, "Instantaneous magnetic field distribution in brushless permanent magnet DC motors. III. Effect of stator slotting," IEEE Transactions on Magnetics, vol. 29, no. 1, pp. 143-151, January 1993.

[4] D. Žarko, D. Ban and T. A. Lipo, "Analytical calculation of magnetic field distribution in the slotted air gap of a surface permanent-magnet motor using complex relative air-gap permeance," IEEE Transactions on Magnetics, vol. 42, no. 7, pp. 1828-1837, July 2006.

[5] A. Tikellaline, K. Boughrara and N. Takorabet, ""Magnetic field analysis of double excited synchronous motor using numerical conformal mapping," in 5th International Conference on Electrical Engineering - Boumerdes (ICEEB), Boumerdes, 2017.

[6] T. C. O'Connel and P. T. Krein, "A Schwarz–Christoffel-based analytical method for electric machine field analysis," IEEE Transactions on Energy Conversion, vol. 24, no. 3, pp. 565-577, September 2009.

[7] F. R. Alam and K. Abbaszadeh , "Magnetic field analysis in eccentric surface-mounted permanent-magnet motors using an improved conformal mapping method," IEEE Transactions on Energy Conversion, vol. 31, no. 1, pp. 333-344, March 2016.

[8] T. Driscoll, "Schwarz–Christoffel Toolbox for MATLAB," 5 June 2019. [Online]. Available: https://tobydriscoll.net/project/sc-toolbox/. [Accessed June 2021].

[9] M. Schröder, A. Ruf, D. Franck, and K. Hameyer, "Einfluss von parasitären Effekten und Fertigungsabweichungen auf die Kräfte in elektrischen Maschinen," e&i Elektrotechnik und Informationstechnik, vol. 134, no. 2, pp. 127–138, 2017.

[10] B. Guo, Y. Huang, F. Peng and J. Dong, "A new hybrid method for magnetic field calculation in IPMSM accounting for any rotor configuration," IEEE Transactions on Industrial Electronics, vol. 66, no. 7, pp. 5015-5024, July 2019.

[11] D. Žarko, D. Ban and T. A. Lipo, "Analytical solution for cogging torque in surface permanent-magnet motors using conformal mapping," IEEE Transactions on Magnetics, vol. 44, no. 1, pp. 52-65, January 2008.

[12] P. Robert, M. Ito and T. Takahashi, "Numerical solution of three dimensional transient eddy current problems by the A- Phi method," IEEE Transactions on Magnetics, vol. 28, no. 2, pp. 116-1169, March 1992.

[13] J. F. Gieras, C. Wang and J. C. Lai, Noise of Polyphase Electric Motors, Taylor & Francis CRC Press, 2005.

[14] J. Le Besnerais, V. Lanfranchi, M. Hequet, G. Lemaire, E. Augis and P. Borchet, "Characterization and Reduction of Magnetic Noise Due to Saturation in Induction Machines," IEEE Transactions on Magnetics, vol. 45, no. 4, pp. 2003-2008, April 2009.

[15] H. Polinder, J. G. Slootweg, J. C. Compter and M. J. Hoeijmakers, "Modelling a linear PM motor including magnetic saturation," 2002 International Conference on Power Electronics, Machines and Drives (Conf. Publ. No. 487), 2002, pp. 632-637.

[16] G. Shrestha, H. Polinder, D. Bang and J. A. Ferreira, "Structural flexibility: A solution for weight reduction of large direct-drive wind-turbine generators," in IEEE Transactions on Energy Conversion, vol. 25, no. 3, pp. 732-740, Sept. 2010.

[17] H. Lan, J. Zou, Y. Xu and M. Liu, "Effect of Local Tangential Force on Vibration Performance in Fractional-Slot Concentrated Winding Permanent Magnet Synchronous Machines," in IEEE Transactions on Energy Conversion, vol. 34, no. 2, pp. 1082-1093, June 2019.

[18] J. Roivainen, Unit-wave response-based modeling of electromechanical noise and vibration of electrical machines, Helsinki University of Technology, 2009

[19] T. B. Sprague, Shape-preserving piecewise cubic interpolation, Western Michigan University, 1990.